===== **ELEMENTARY PARTICLES AND FIELDS** =====
Experiment

Investigation of the Deuteron Spin Structure at Short Nucleon−Nucleon Distances in the Reaction of Polarized-Deuteron Fragmentation to Cumulative Pions

**L. S. Azhgirey[†], S. V. Afanasiev, Yu. T. Borzounov, L. B. Golovanov, L. S. Zolin[*],
V. I. Ivanov, A. Yu. Isupov[**], V. P. Ladygin, A. G. Litvinenko, A. I. Malakhov, V. N. Penev,
V. F. Peresedov, Yu. K. Pilipenko, S. G. Reznikov, P. A. Rukoyatkin, and A. N. Khrenov**

Joint Institute for Nuclear Research, Dubna, Moscow oblast, 141980 Russia
Received October 12, 2010

Abstract—Experimental results on the vector (A_y) and tensor (A_{yy}) analyzing powers in the fragmentation of 5- and 9-GeV/c polarized deuterons to high-momentum pions in the kinematical region corresponding to pion production on a strongly correlated nucleon pair (cumulative meson production) are presented. The angular and momentum dependences of A_{yy} are not described by calculations performed in the impulse approximation by using standard deuteron wave functions. An explanation for our data should be sought on the basis of models that treat the deuteron at short distances (deuteron-core region) as a multiquark state—for example, a $6q$ cluster, whose high orbital angular momentum (D wave) leads to the observed strong dependence of the reaction tensor analyzing power $A(\vec{d}, \pi)X$ on the pion transverse momentum.

1. INTRODUCTION

Investigation of the deuteron-core structure with allowance for spin degrees of freedom provides a key to obtaining deeper insight into the structure of nuclear forces at short distances. This is one of the intricate problems in strong-interaction physics—without solving this problem, it is impossible to explain the properties of nuclear matter as such and special features of the nuclear structure that manifest themselves in the form of collective effects under conditions where a group of nucleons forms a cluster of strongly correlated particles. Evidence in support of the presence of such clusters in nuclei was obtained in 1957 at the synchrocyclotron of the Joint Institute for Nuclear Research (JINR, Dubna) in experiments devoted to studying the direct knockout of deuterons from nuclei undergoing quasielastic interaction with incident protons, the energy transfer to a nucleon pair being two orders of magnitude higher than the nucleon binding energy in the deuteron [1]. In order to explain the results of those experiments, D.I. Blokhintsev [2] proposed the model of fluctons, which are fluctuations of the nuclear-matter density.

Blokhintsev put forth the flucton hypothesis long before the discovery of the quark structure of hadrons.

A key role of analyzing the structure of the deuteron core as a proton−neutron flucton in exploring the flucton component in nuclei was highlighted [3−5] in implementing experiments devoted to studying cumulative reactions and initiated after the formulation of A.M. Baldin's hypothesis of the cumulative effect in the fragmentation of relativistic nuclei [6].

The cumulative-effect hypothesis was based on extending the hypothesis of a limiting fragmentation of particles at high energies [7] to the interaction of relativistic nuclei. Both hypotheses assume a decisive role of the constituent nature of the fragmenting particle in interaction dynamics.

A description of nucleon fragmentation is based on the parton model developed by R.P. Feynman and J.D. Bjorken for analyzing particle interactions at high energies. Baldin indicated that, at rather high energies, nucleon degrees of freedom in nuclei become inadequate, since partons, which are constituents of nucleons, begin manifesting themselves as quasifree particles, so that the nucleus behaves as a parton gas rather than as a nucleon gas. In view of this, partons of the nucleus begin forming the spectrum of secondaries in the fragmentation of

[†]Deceased.
[*]E-mail: `zolin@sunhe.jinr.ru`
[**]E-mail: `isupov@moonhe.jinr.ru`

nuclei in just the same way as in nucleon fragmentation. A scale invariance of the spectra of secondaries is a feature peculiar to the regime of limiting fragmentation. This invariance consists in the following: the longitudinal-momentum spectra of target fragments cease to be dependent on the projectile energy and quantum numbers, reflecting the internal constituent nature of the fragmenting particle. The scale-invariant behavior of the spectra manifests itself if one represents these spectra as a function of the scaling variable x_F (Feynman variable [8]), which is proportional to the ratio of the longitudinal momentum of a secondary particle in the c.m. frame, $P_{c.m.\parallel}$, to the total interaction energy in the same reference frame, $x_F = 2P_{c.m.\parallel}/\sqrt{s}$. The second, frequently used, definition of the Feynman variable is $x_F = P_{c.m.\parallel}/P_{c.m.\parallel}^{max}$, where $P_{c.m.\parallel}^{max}$ is the maximum kinematically allowed longitudinal momentum of a particle; in this case, the variable x_F ranges between -1 and 1 [9]. In nucleon fragmentation, the variable x_F is related by a simple equation to the fragment energy E_c and momentum P_c in the laboratory frame; that is,

$$x_F = 2P_{c.m\parallel}/\sqrt{s} = \frac{E_c - P_c \cdot \cos(\theta)}{m_N} \simeq x_c, \quad (1)$$

where x_c stands for a cumulative number. The cumulative variable x_c was proposed by Baldin and Stavinsky as a scaling variable in describing the spectra of nuclear fragments [10–12]. The definition of x_c is based on the condition requiring that the 4-momentum of the system of interacting particles be conserved in the inclusive reaction $a + b \to c + X$ involving the production of a cumulative fragment c, provided that the mass of the hadronic residue X is minimal.

In expression (1), the denominator involves the nucleon mass m_N; we also have $x_F^{max} = 1$. If the fragmenting mass is larger than m_N, then $x_F^{max} > 1$, provided that m_N remains in the denominator. In this case, x_F^{max} shows how many times the fragmenting mass must exceed the nucleon mass for the production of a particle that has the measured value of $P_{c.m.\parallel}$ to be possible. The above treatment of the cumulative number x_c as the minimum fragmenting mass (in units of m_N) follows from its definition. Relation (1) is convenient for estimating x_c under the condition $m_c \ll \sqrt{s}$. The difference between x_F and x_c (the latter being defined according to [11, 12]) is modest and decreases fast with increasing energy: $\Delta x_{F,c} \leq$ 8% at $\sqrt{s} = 4$ GeV and $\Delta x_{F,c} \leq 2\%$ at $\sqrt{s} = 8$ GeV (see [13], Appendices A and B).

In the deuteron-fragmentation reaction on target nucleons that is studied here and which is accompanied by the escape of pions at an angle θ,

$$d + N \to \pi(\theta) + X,$$

the variable x_c is determined by the relations

$$x_c = \frac{(p_N p_\pi) - m_\pi^2/2}{(p_d p_N) - (p_d p_\pi) - m_N^2}$$

$$= \frac{2E_\pi m_N - m_\pi^2}{E_d m_N - E_d E_\pi + \mathbf{P}_d \mathbf{P}_\pi - m_d m_N} < 2,$$

where p_i is the 4-momentum of particle i and m_i, E_i, and $\mathbf{P}_i$ are its mass, total energy, and 3-momentum (in the laboratory frame), respectively.

We have dwelled at length on the limiting-fragmentation hypothesis, Feynman scaling, the cumulative-effect hypothesis, and the use of the scaling variables x_F and x_c in order to highlight the common nature of approaches in studying the mechanism of the fragmentation of high-energy nucleons and the mechanism of the fragmentation of relativistic nuclei. The involvement of parton mechanisms and quark−gluon degrees of freedom in nucleons and nuclei is a common feature here. The cumulative effect is determined by the collectivization of quarks in correlated intranuclear nucleons (fluctons), where the momentum distribution of partons, which is characterized by the Bjorken variable x_B [14], goes beyond the limiting value of $x_B = 1$ admissible for free nucleons. A cumulative number above unity $(x_c > 1)$, in just the same way as a value of the Bjorken variable above unity $(x_B > 1)$, is indicative of this excess.[1]

The fact that the spectra of cumulative particles produced with a low transverse momenta do not depend on the interaction energy or on the probe sort (h, l, γ) is an argument in support of the dominance of the spectator mechanism of cumulative-particle production—that is, the hadronization of a spectator quark produced upon the probe-induced breakup of a multiquark configuration in nucleus A, where h, l, or γ may play the role of a probing particle; that is,

$$h(l, \gamma) + A \to h_c + X. \quad (2)$$

In the 1970s and 1980s, intensive investigations of cumulative processes were performed by

---

[1] In the region of very high 4-momentum transfers q, in which case one can disregard particle masses, the variable x_c transforms into the Bjorken variable x_B, which characterizes that fraction of the 4-momentum of the intranuclear nucleon at rest which the interacting parton carries in the deep-inelastic-scattering reaction $e + A \to e' + X$ [10, 12],

$$x_c = -\frac{\frac{1}{2}(p_e - p_{e'})^2}{(p_e p_N) - (p_N p_{e'})} = -\frac{q^2}{2(p_N q)} = x_B.$$
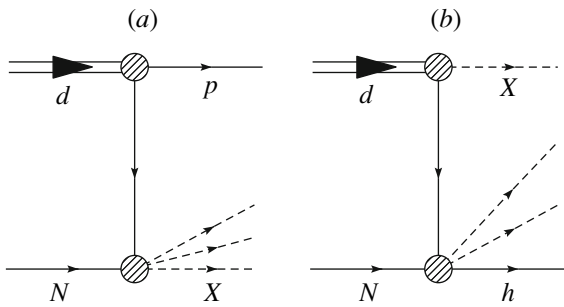
Fig. 1. Impulse-approximation diagrams for deuteron fragmentation on a nucleon, $d + N \to h + X$: (a) spectator diagram for the stripping reaction $d + N \to p(0°) + X$ and (b) diagram for the direct mechanism in deuteron fragmentation to a hadron $h = n, p, \pi, K, \ldots$. The solid lines correspond to observed particles.

Baldin and his colleagues at the synchrophasotron in Dubna [11, 12], G.A. Leksin and his colleagues at the Institute of Theoretical and Experimental Physics (ITEP, Moscow) [15], and physicists from Berkeley [16]. All relevant experiments, including those performed at higher energies at the Institute for High Energy Physics (IHEP, Protvino) [17] and the Fermi National Accelerator Laboratory (Chicago, USA)[18, 19], confirmed the scale-invariant behavior of cumulative spectra that is characteristic of the limiting-fragmentation regime. In accordance with relation (1), the shape of the spectra of cumulative particles whose mass m_c is much lower than the interaction energy $\sqrt{s}$ proved to be only slightly dependent in the reference frame comoving with the fragmenting nucleus on the choice of one of the variables x_c, P_c, and E_c. In the experiments performed in Dubna, experimental data were represented as a rule versus the invariant variable x_c, which is convenient for use both in the case of the fragmentation of target nuclei and in the case of the fragmentation of relativistic nuclei. In the present article, we will use a representation in terms of the variable x_c.

One of the alternative mechanisms that is able to provide quantitative estimates for the yield of cumulative particles is based on the nucleon model of the nucleus and the use of the impulse approximation (see Fig. 1). In this approach, nucleons are treated as quasifree particles whose internal motion in the nucleus is characterized by the Fermi momentum. In this case, the production of a cumulative meson becomes possible owing to the interaction of a high-momentum nucleon from the fragmenting nucleus with a target nucleon, $NN \to NN\pi X$ (in the following, this mechanism is referred to as a direct mechanism). The presence of a high-momentum component in a nucleus is explained by the existence of short-range few-nucleon correlations between two or more nucleons [20, 21]. As the nucleon–nucleon

spacing r_{NN} decreases, the momentum of relative motion in a correlated nucleon pair increases and may reach values above 0.5 GeV/c for $r_{NN} < 0.4$ fm— that is, in the case of a significant overlap of nucleon wave functions. This interpretation of few-nucleon correlations, where nucleon wave functions overlap and where the nucleon mass becomes indefinite because of off-shellness as the momentum of relative motion increases, complies poorly with the impulse-approximation pattern, where the nucleons are quasifree and where one ignores their size and internal structure. Therefore, it is natural to expect that only in the realms of nuclear reactions, where internal momenta do not exceed 300 MeV/c, can one hope for a successful application of the impulse approximation. Nevertheless, attempts at employing the impulse approximation at high momenta are justified by the fact that, at the present time, this is the only available formalism that, given the nuclear wave function, makes it possible to obtain quantitative predictions for the behavior of observables in the fragmentation of nuclei.

The model of multiquark configurations in nuclei underlies yet another popular approach based on the idea of fluctons. This model was successfully applied to interpreting experiments devoted to studying cumulative reactions [22, 23]. The approach in question seems more promising in studying fluctons, since it provides an interpretation of their internal structure in terms of quark degrees of freedom in nuclei. The validity of the approach based on the multiquark-configuration model was confirmed by data of the European Muon Collaboration (EMC) [24]. Those data revealed that the nuclear quark-parton structure functions differ from the free-nucleon structure functions. A weak dependence of the momentum spectra of cumulative particles on the interaction energy, the cumulative-fragment sort (π, K, p), and the probe type (h, l, γ) is naturally explained within the multiquark-configuration model under the assumption of the spectator mechanism of cumulative-particle production in flucton breakup.

Neither of the two models (few-nucleon correlation and multiquark configurations) is able to explain successfully all known special features of cumulative reactions. By way of example, we indicate that, within the multiquark-configuration approach, it is difficult to explain a strong excess of the proton yield in relation to the yield of mesons ($p/\pi \geq 10^2$) of the same momentum in reactions belonging to the type in (2) [25]. Models of few-nucleon correlations associate this fact with a high probability of flucton dissociation to nucleon fragments. At the same time, no nucleon model of the nucleus is able to explain an approximate invariability with increasing x_c of the particle-to-antiparticle yield ratios (K^+/K^- and

$\pi^-/\bar{p}$) in cumulative reactions in contrast to their fast variations in nucleon—nucleon (NN) interactions in response to the growth of the invariant variable x_F. In [26], this feature of flucton fragmentation is explained by the presence of a harder $q\bar{q}$ sea in fluctons (heavy-multiquark-formation model based on the formalism of quark—gluon strings). In all models associated with considering special features of a quark sea in fluctons, there is a want of more precise data on the yield of cumulative antiparticles in deuteron fragmentation.

Being the simplest nucleus, the deuteron provides a unique possibility for studying the properties of fluctons. For more than half a century, the structure of the deuteron has been studied by using all types of probes (photons, leptons, and hadrons), but some details of the structure of the deuteron wave function at short distances still remain unclear. Within the mutiquark-configuration approach, the structure of the deuteron core at nucleon—nucleon distances smaller than the nucleon size ($r_{NN} < 0.7$ fm) can be studied as a six-quark ($6q$) configuration with allowance for quark—gluon degrees of freedom and with the aid of information about the internal structure of nucleons. Even at the initial stage of studying the cumulative effect [3—5, 27], many authors indicated that this approach is promising.

Investigation of multiquark configurations in the deuteron has obvious advantages in relation to studying them in more complex nuclei, since, in the former case, there is no distorting effect of nuclear matter on the properties of products of multiquark-configuration fragmentation. However, rescattering and absorption on the constituents of a multiquark configuration may occur after primary interaction. This is so for any sorts of probes.

An extensive program of investigations into the deuteron structure at short distances (deuteron core) is being performed in high-energy photon and electron beams. This paves the way toward the employment of pointlike probes. In the case of applying hadron probes, this is impossible—the cross section for the process being considered depends on both the target and projectile structure functions, and this complicates greatly the interpretation of respective results. However, large cross sections for strong-interaction processes render hadron probes highly advantageous when it is necessary to penetrate the region of very short nucleon—nucleon distances r_{NN}.

Because of a fast reduction of cross sections in the cumulative region with increasing x_c, information about nuclear structure functions in this region from deep-inelastic lepton scattering was scanty until recently. The data were obtained in μC [28] and νFe [29] scattering only in the x_B region extending up to 1.2. At the same time, the momentum spectra of pions from the reaction of deuteron fragmentation to cumulative pions, $dp \to \pi X$, were studied up to a value of $x_c \simeq 1.8$, which is close to the kinematical limit of $x_c = 2$. An additional advantage of studying the deuteron at short distances as a multiquark configuration is that the spin structure of such a configuration has two components characterized by the orbital angular momenta of $L = 0$ and 2. In principle, this may provide the possibility of studying the role of the orbital nucleon-spin component in the formation of the spin structure of the deuteron core as a proton—neutron flucton.

Investigation of the spin structure of fluctons in $A > 2$ nuclei is likely to be a problem for the future, but the way toward solving it obviously depends on successes in obtaining deeper insight into the structure of the deuteron as a $6q$ flucton of isotopic spin equal to zero. Recent measurements performed at the Thomas Jefferson Laboratory (JLab)[30] revealed that, in $A > 4$ nuclei, about 20% of the nucleons enter into the composition of NN fluctons, of which 90% are in the $I = 0$ isotopic state—that is, they are deuteron-like objects. This composition of fluctons is due to the presence of a tensor component in NN potentials [31].

The possibility of studying the spin structure of the deuteron core in $\vec{d}A$ interactions appeared after the advent of beams of relativistic polarized deuterons whose energy exceeded 1 GeV per nucleon. In the 1990s, experiments at the accelerators in Dubna (synchrophasotron, $P_d \leq 9$ GeV/c) and Saclay (Saturn-2, $P_d \leq 3.5$ GeV/c) were performed in order to measure the tensor analyzing power T_{20} in $A(\vec{d}, p)X$ stripping reactions [32—35] and in the elastic-backscattering process $p(\vec{d}, p)d$ [36, 37], as well as to measure polarization transfer from a deuteron to a proton in processes of the $A(\vec{d}, \vec{p})X$ type [38—40].

We assume that the spectator diagram (Fig. 1) is dominant in $A(\vec{d}, p)X$ and $A(\vec{d}, \vec{p})X$ inclusive reactions and that the one-nucleon-exchange diagram is dominant in the reaction $p(\vec{d}, p)d$. The impulse approximation seems applicable to these reactions. However, only at low internal momenta in the deuteron did experimental data prove to be in agreement with the results of calculations performed in the impulse approximation with standard deuteron wave functions [41—45]. In Fig. 2, data on T_{20} for $A(\vec{d}, p)X$ and $p(\vec{d}, p)d$ processes are shown versus the internal momentum k defined within line-front
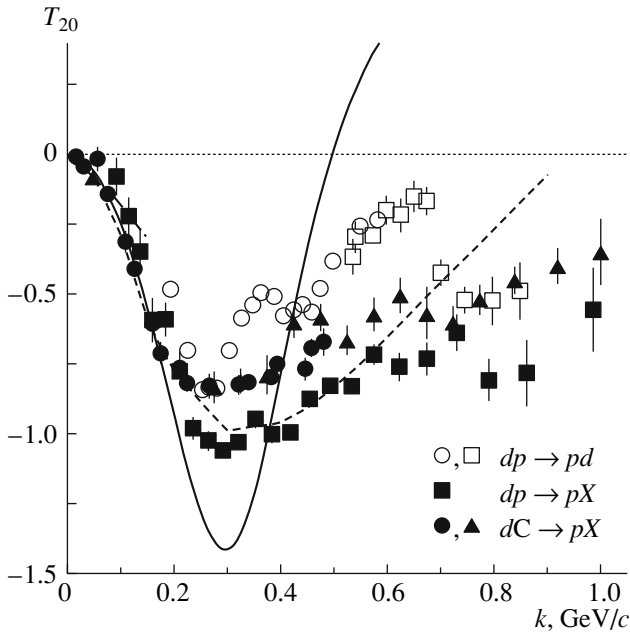
Fig. 2. Data on the tensor analyzing power T_{20} versus the internal momentum k for the $dA \to pX$ deuteron-breakup reactions [32−34] on hydrogen and carbon targets and for the elastic-backscattering reaction $dp \to pd$ [36, 37]. The solid curve represents T_{20} calculated in the impulse approximation with the Paris deuteron wave function [41]; the calculated behavior of T_{20} is similar for the two reactions in question. The dashed curve stands for $T_{20}(k)$ calculated for $dA \to pX$ with allowance for final-state interaction [47].

dynamics.[2)] At k values above 0.3 GeV/c, there is a discrepancy with the results of the calculations in the impulse approximation, and this discrepancy grows with increasing k.

The character of deviations is different for the different reactions, suggesting different contributions from nonspectator diagrams disregarded in the calculations based on the two-vertex diagrams. The

---

[2)]In the fragmentation of relativistic deuterons, the measured momentum of the nucleon appearing as a fragment, P_p, is used to determine the internal momentum in the deuteron, k, in accordance with the rules of light-front dynamics (see, for example, [25, 46]); that is,

$$\mathbf{k}^2 = \frac{m_\perp^2}{4\alpha(1-\alpha)} - m_p^2, \qquad m_\perp^2 = \mathbf{k}_\perp^2 + m_p^2, \quad (3)$$

where $\mathbf{k}_\perp$ is the proton transverse momentum and $\alpha = (E_p + P_p)/(E_d + P_d)$ is the light-front variable determining the deuteron-momentum fraction carried away by the proton in the infinite-momentum frame (here, E_p and E_d are the total energies of the proton and deuteron, respectively). The momentum k is used in analyzing relativistic bound states—in particular, in constructing relativistic deuteron wave functions. Up to values between 0.2 and 0.3 GeV/c, k is close to the internal nucleon momentum in the deuteron rest frame.

inclusion of the additional contribution from three-vertex diagrams (effects of rescattering, absorption, and final-state interaction) makes it possible to improve the description of data up to $k \simeq 0.6$ GeV/c [47, 48]. At higher k, part of the data can be described by phenomenologically introducing a $6q$ component, its strength in the deuteron wave function being chosen parametrically [47, 49].

The obvious need for the inclusion of relativistic effects for $k > 0.3$ GeV/c initiated searches for adequate forms of taking into account relativistic corrections. However, the introduction of additional P-wave components of the deuteron wave function within the relativistic nucleon model of the deuteron [50−52] did not remove completely discrepancies with experimental data. The possible manifestation of three-nucleon forces in employing a nucleon probe with the aim of exploring a strongly correlated NN system has not yet been considered.

The example of the aforementioned theoretical studies shows that the use of the impulse approximation without going beyond nucleon−meson degrees of freedom (NN potentials of the types in [41−43, 45]) is insufficient for obtaining a satisfactory description of polarized-deuteron fragmentation on nuclei that is accompanied by the emission of cumulative fragments in the form of nucleons. This is indicative of the possible inadequacy of employing, at short distances in the deuteron, NN potentials obtained from experiments with free nucleons and suggests a significant contribution of secondary processes involving a nucleon as a fragment, which complicate the derivation of information about the amplitude associated with the primary elementary process and determined by the structure of the proton−neutron flucton. This also indicates that it is necessary to develop theoretical and experimental approaches to studying the spin structure of the deuteron core with allowance for its multiquark structure and to explore reactions involving the production of more appropriate fragments—that is, mesons whose quark structure is simpler than that of nucleons and which also make it possible to obtain information about the role of sea quarks in the formation of fluctons. In the present study, we describe relevant experiments and present results obtained in polarized beams at the Laboratory of High Energies at JINR in studying spin effects in reactions of the $A(\vec{d}, \pi)X$ type.

2. DESCRIPTION OF THE EXPERIMENT

2.1. Analyzing Powers in $A(\vec{d}, h)X$ Reactions Involving Polarized-Deuteron Fragmentation

In describing polarization effects in reactions involving a vector particle, one employs polarization parameters that, depending on the choice of coordinate

basis, are expressed in terms of tensor components either in the spherical [53] or in the Cartesian [54] representation. It is generally accepted (Madison convention [55]) that, in experiments with beams of polarized particles, the system of coordinates is chosen in such a way that the z and y axes are directed along, respectively, the beam axis and the normal to the reaction plane. In experiments with an accelerated beam of polarized deuterons, it is additionally

required that the spin-quantization axis be orthogonal to the plane of the accelerator orbit and, hence, to the beam axis. If this condition remains valid in transporting the beam to the target (the z projection of the deuteron spin is zero), then terms that depend on the z projection of the spin vanish in the cross section as a function of polarization parameters. In this case, the differential cross section $\sigma(\theta, \phi)$ for a reaction with polarized deuterons can be written as

$$\sigma(\theta, \phi) = \sigma_0(\theta) \left[1 + \sqrt{2}\rho_{10} iT_{11}(\theta) \cos \phi - \frac{1}{2}\rho_{20} T_{20}(\theta) - \sqrt{\frac{3}{2}}\rho_{20} T_{22}(\theta) \cos 2\phi \right],$$

$$\sigma(\theta, \phi) = \sigma_0(\theta) \left[1 + \frac{3}{2} A_y(\theta) p_z \cos \phi + \frac{1}{4} p_{zz} \left(A_{yy}(\theta)(1 + \cos 2\phi) + A_{xx}(\theta)(1 - \cos 2\phi) \right) \right]$$

if use use is made of, respectively, the spherical and the Cartesian representation of polarization parameters [56]. Here, $\sigma_0(\theta)$ is the differential cross section for unpolarized deuterons; θ and ϕ are, respectively, the polar and azimuthal angles of detected-particle emission (ϕ is reckoned from the plane spanned by the incident-deuteron momentum and the axis of deuteron-spin quantization); and the parameters $\rho_{10} = \sqrt{\frac{3}{2}}p_z$ and $\rho_{20} = \sqrt{\frac{1}{2}}p_{zz}$ are related to the vector (p_z) and tensor (p_{zz}) components of the beam polarization in the reference frame where the quantization axis is aligned with the symmetry axis. In the chosen coordinate frame, the analyzing powers in the spherical [vector (iT_{11}) and tensor (T_{20} and T_{22}) ones] and Cartesian [vector (A_y) and tensor (A_{xx} and A_{yy}) ones] representations are related by the equations

$$A_y(\theta) = \frac{2}{\sqrt{3}} iT_{11}(\theta),$$

$$A_{xx}(\theta) = -\sqrt{2} \left[\frac{1}{2}T_{20}(\theta) - \sqrt{\frac{3}{2}}T_{22}(\theta) \right],$$

$$A_{yy}(\theta) = -\sqrt{2} \left[\frac{1}{2}T_{20}(\theta) + \sqrt{\frac{3}{2}}T_{22}(\theta) \right].$$

In the case of observation at zero angle ($\theta = 0°$), T_{20} and A_{yy} are related by the simple equation $T_{20} = -\sqrt{2}A_{yy}$, and a comparison of data from relevant experiments where use is made of the different representations is facilitated owing to this. If $\phi = 0$, as is the case in our experiment (the reaction and orbit planes are coplanar), then the cross section for various signs of the deuteron polarization ($\pm, 0$) has the

simplest form in the Cartesian representation, where only two terms involving the vector (A_y) and tensor (A_{yy}) analyzing powers survive; that is,

$$\sigma^{\pm}(\theta) = \sigma_0(\theta) \left[1 + \frac{3}{2} A_y(\theta) p_z^{\pm} + \frac{1}{2} A_{yy}(\theta) p_{zz}^{\pm} \right].$$

In this case, A_y and A_{yy} are calculated in terms of the particle yields N^+, N^-, and N^0 normalized in the deuteron-beam intensity. This is done by using the relations

$$A_y(\theta) = \frac{3}{2} \cdot \frac{p_{zz}^+(N^-/N^0 - 1) - p_{zz}^-(N^+/N^0 - 1)}{p_z^- p_{zz}^+ - p_z^+ p_{zz}^-}, \tag{4}$$

$$A_{yy}(\theta) = -2 \cdot \frac{p_z^+(N^-/N^0 - 1) - p_z^-(N^+/N^0 - 1)}{p_z^- p_{zz}^+ - p_z^+ p_{zz}^-}. \tag{5}$$

In our experiments, the systematic errors in measuring A_y and A_{yy} were associated primarily with inaccuracies in information about the beam polarization and were about 5%.

2.2. Implementation of the Experiment

Our measurements were performed in a beam of polarized deuterons extracted from a ring accelerator by means of a slow-extraction system, which ensured a uniform intensity of a beam with a momentum of up to 9 GeV/c for 0.5 s. In the case of employing the Polaris cryogenic source of polarized deuterons [57], a typical intensity of the extracted beam was 1.5×10^9 deuterons per acceleration cycle (10 s). The POLARIS source can operate in the regime of a vector or a tensor polarization, depending

Table 1. Theoretical values of the vector (p_z) and tensor (p_{zz}) polarizations of deuterons from the POLARIS source

High-frequency transition	p_z	p_{zz}
1–4	$-2/3$	0
3–6	$+2/3$	0
2–6	$+1/3$	$+1$
3–5	$+1/3$	-1
High-frequency field off	0	0

on the type of the transition induced by a high-frequency field between the levels of the deuterium hyperfine structure in a magnetic field. Four types of high-frequency transitions are used in the source. The theoretical values of the vector (p_z) and tensor (p_{zz}) polarizations of the deuterons are presented in Table 1 for the case where the atomic deuterium beam does not contain atoms unpolarized in the electron spin.

Typical values of the deuteron polarization measured under conditions of injection to the ring accelerator in the vector and tensor regimes of source operation are $p_z = 0.52 \pm 0.02$ and $p_{zz} = 0.75 \pm 0.05$, respectively. By appropriately going over from one type of high-frequency transitions to another, a positive, zero, and a negative value of the polarization ($+$, 0, $-$) are made to follow one another circularly in each mode from one cycle to another, whereby the errors associated with the drift of the magnitude of each-sign polarization are reduced to a minimum upon averaging over many cycles.

In order to form an atomic beam and to maintain a vacuum at a level of $\simeq 10^{-7}$ mbar, the process of a cryogenic pumping is used in the POLARIS pulsed source: upon the injection of each portion of deuterium, its scattered part is frozen out at surfaces having liquid-helium temperature (4.2 K). Flows of background hydrogen and hydrocarbon vapors diffusing from the linac into the source are precipitated at the surfaces. The level of the deuteron-beam polarization decreases by 10 to 15% after many days of source operation. Possibly, this is due to the sublimation and ionization of frozen admixtures.

In order to monitor polarizations, we used a set of polarimeters. The polarization at the linac outlet at an energy of 10 MeV was measured with a low-energy polarimeter (LEP) equipped with semiconductor detectors [58]. Vector and tensor polarizations were tested by studying, respectively, the asymmetry of the alpha-particle yield in elastic $\vec{d} + {}^4\text{He}$ scattering and the change in the cross section for the reaction $\vec{d} + {}^3\text{He} \rightarrow p(0°) + {}^4\text{He}$. In test measurements of the

deuteron polarization in the slow-extraction channel, we employed the ALPHA two-arm polarimeter [59], which measured the asymmetry in elastic deuteron scattering on hydrogen at an angle of 7.5° for the deuteron momentum of $P_d = 3.0$ GeV/c. The vector (A_y) and tensor (A_{yy}) analyzing powers known for this process to a high precision [60] ensure a small systematic error in measuring the vector and tensor polarizations of the beam, $\Delta p_z = 0.03$ and $\Delta p_{zz} = 0.025$. The readings of the polarimeter before injection into the ring accelerator were in good agreement with the readings of the polarimeter in the slow-extraction channel. This confirms the absence of depolarization effects in the acceleration of deuterons to a momentum of 9 GeV/c.

In order to test the degree of vector polarization averaged over the time of each exposure, we used a polarimeter featuring a thin polyethylene target and measuring the asymmetry of quasielastic proton–proton scattering [61]. The CH_2 polarimeter was placed at one of the intermediate foci of the slow-extraction channel upstream of the working-target position. In the tensor mode of POLARIS operation, the CH_2 polarimeter was used to measure the vector component p_z in the deuteron beam. This component proved to be about $1/3$ of p_{zz} (see Table 1). In measuring fragment yields at nonzero angles, this made it possible to obtain data both on the tensor (A_{yy}) and on the vector (A_y) analyzing power in accordance with relations (3) and (4).

Our investigation of spin effects in $\vec{d} + A \rightarrow (p, \pi) + X$ inclusive reactions at fragment-escape angles of up to 180 mrad was performed with the aid of a focusing spectrometer (see Fig. 3). A deuteron beam extracted from the accelerator was directed to the target placed at the focus F5 of the channel of slow extraction from the synchrophasotron. Particles of preset momentum were selected by a spectrometer consisting of a set of dipoles and quadrupoles over a length of about 50 m in the 4V secondary-particle channel.

In studying $A(\vec{d}, \pi)X$ reactions, we employed liquid-hydrogen, beryllium, and carbon targets ($A = 1$, 9, and 12). In choosing targets, we took into account the following circumstances. In studying the deuteron structure via fragmentation on a target nucleon, it is desirable to employ a hydrogen target in order to avoid the effect of secondary interactions in target nuclei and rescattering in high-density targets on the properties of fragments. At the same time, very small cross sections for cumulative reactions involving the production of high-momentum pions make one increase the thickness of targets. The effect of the target atomic number and thickness was studied in detail in $A(\vec{d}, p)X$ inclusive cumulative reactions.
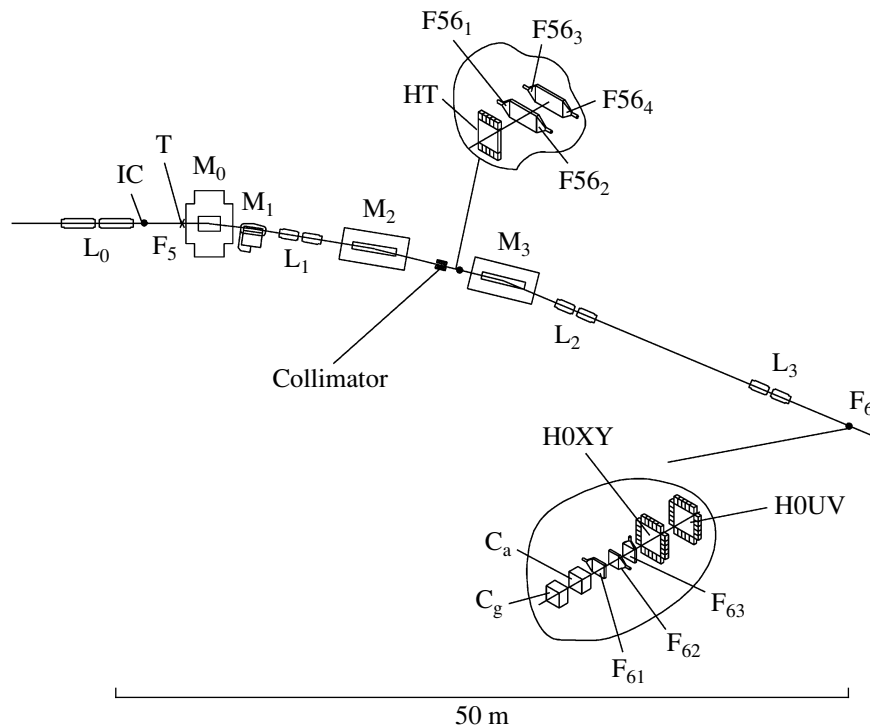
Fig. 3. Layout of the focusing spectrometer in the 4V channel (the distance between the foci F_5 and F_6 is about 50 m): (M_i) magnets; (L_i) doublets of quadrupole lenses; (IC) ionization chamber; (T) target at the focus F5 of the slow-extraction channel; (F_{61}, F_{62}, and F_{63}) triggering scintillation counters; ($F56_{1-4}$) scintillation counters at the intermediate focus upstream of the collimator; (HT) scintillation hodoscope for time-of-flight measurements; (H0XY and H0UV) beam-profile hodoscopes at the focus F6; and (C_g and C_a) gas and aerogel threshold Cherenkov counters, respectively.

It was found that the A dependence of the tensor analyzing power T_{20} manifests itself at high internal momenta in the deuteron (in excess of 0.2 GeV/c) and that only for light nuclei of mass number A in the range between 1 and 4 does the tensor analyzing power itself have sizable values [32–34]. Upon the replacement of a hydrogen target by a helium one, T_{20} decreases by 20%. For still greater values of the target atomic number ($A > 4$), the A dependence is weak. Since the analyzing power is defined in terms of the cross-section ratio $\sigma_{pol}/\sigma_{unpol}$, the results of the measurements change only slightly in response to an increase in the target thickness Δ_T. With allowance for weak A and Δ_T dependences, basic measurements of spin effects in $A(\vec{d}, \pi)X$ reactions were performed with a beryllium target 36 g/cm^2 in thickness. For test measurements, we employed a 1-m (7-g/cm^2) liquid-hydrogen target [62] and a carbon target 55 g/cm^2 in thickness.

The beam dimensions over the slow-extraction channel were monitored by profilometers (multiwire proportional chambers). Typical beam dimensions at the focus F5 were $\sigma_x = 4$ mm and $\sigma_y = 9$ mm. The forward objective of the focusing spectrometer (see Fig. 3) in the form of a doublet of quadrupole

lenses L_1 was at a distance of 6 m from the target, and this restricted the spectrometer acceptance in the polar angle to ± 8 mrad. The spectrometer acceptance in the solid angle was $\Delta\Omega \simeq 0.9 \times 10^{-3}$ sr. The H0XY and H0UV scintillation hodoscopes 16×16 cm^2 in size (16 elements of size 16×1 cm^2 in each plane) were used to monitor the beam dimensions and position at the ultimate focus F6. In the case of employing thick targets, the beam dimensions at F6 were $\sigma_x \simeq \sigma_y = 20$ mm.

In the working momentum range of the spectrometer between 1.5 and 6 GeV/c, the momentum acceptance was $\Delta p/p \simeq 2\%$, on average. The total acceptance $\Delta\Omega\Delta p/p$ changed in response to changes in the momentum tuning of the channel. The magnitude of this acceptance was determined for all preset momentum values and particle types via a Monte Carlo simulation by using the BELIM [63] and GEANT3 [64] packages. In this simulation, we took into account particle losses because of nuclear interaction and multiple scattering in matter along the 4V channel. For unstable particles, we also took into account losses because of their finite lifetime.

In addition to the measurements with the polarimeters, the tensor polarization of the primary
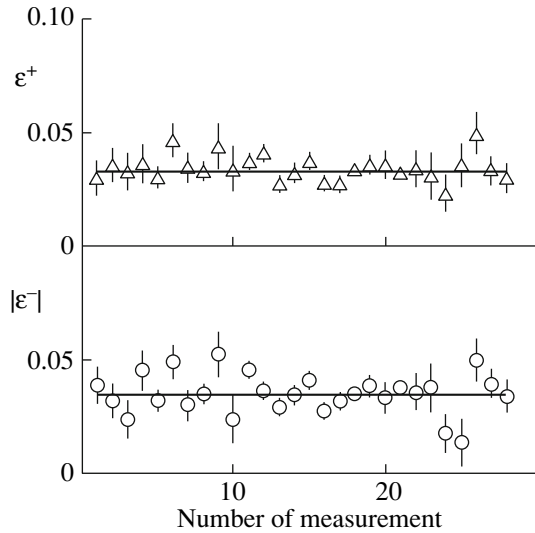
Fig. 4. Left−right asymmetries $\varepsilon^{\pm}$ of the proton yield in $\vec{d} + CH_2 \rightarrow p + X$ reactions according to measurements with a double-arm polarimeter in a beam of tensorially polarized deuterons [61].

deuteron beam was tested at regular intervals directly by the focusing spectrometer with the aid of the procedure based on the use of the well-known tensor analyzing power T_{20} for $A(\vec{d}, p)X$ reactions in the case of proton emission at zero angle. Previously, it was shown in [65] that, in detecting protons of momentum $P_p = \frac{2}{3}P_d$, the analyzing power T_{20} was -0.82 ± 0.04 and did not depend on the target atomic number in the region $A > 4$ or on the deuteron momentum in the range from 2.5 to 9.0 GeV/c. At $\theta_p = 0°$ and known T_{20}, the tensor analyzing power of the beam is determined by the simple relation

$$p_{zz}^{\pm} = \frac{2}{\sqrt{2}} T_{20} \left(1 - \frac{N^{\pm}}{N^0} \right),$$

where $N^{\pm}$ and N^0 are normalized proton yields for respective deuteron polarizations.

The polarimeter featuring a thin polyethylene target provided the possibility of monitoring the vector component of the deuteron polarization. The magnitude of the polarization was calculated from the asymmetry of quasielastic proton−proton scattering at an angle of 8°. Figure 4 shows the results obtained by measuring the left−right asymmetry of proton−proton scattering at the deuteron momentum of 9 GeV/c over a period of about three days [61]. The vector-component values averaged over this period for the positive and negative tensor modes of source operation were $p_z^+ = 0.275 \pm 0.016(\text{stat.}) \pm 0.014(\text{syst.})$ and $p_z^- = 0.287 \pm 0.016(\text{stat.}) \pm 0.014(\text{syst.})$, respectively.

The time-of-flight technique was the main means for identifying particles that reached the ultimate focus F6 of the spectrometer. The scintillation counters $F56_i$ and $F6_i$ (see Fig. 3) of the time-of-flight system were positioned in such a way as to form the flight bases of length 27 and 21 m. Event selection with the aid of a correlation of two times of flight (TOF1 and TOF2) made it possible to suppress the background of random coincidences substantially. In tuning the spectrometer to detecting negatively charged particles, the time-of-flight technique made it possible to select reliably pions almost over the entire working range of momenta. The need for additionally employing threshold Cherenkov counters arose in detecting positively charged particles of momentum in excess of 3.0 GeV/c, since the number of protons in the beam exceeded considerably the number of mesons (by three orders of magnitude at a momentum of 4 GeV/c). In order to suppress signals from protons, signals from Cherenkov counters were introduced in the trigger scheme. Use was made of counters of two types: that featuring a gaseous radiator (N_2, 10 atm) and that featuring an aerogel radiator (SiO_2, $n = 1.014$). Figure 5 demonstrates the suppression of protons in the correlation spectrum upon the inclusion of one gas-filled counter and both counters in the event-selection scheme. The proton-suppression coefficient was 200 and 3000, respectively.

3. RESULTS OF THE MEASUREMENTS

The analyzing powers $T_{20}(\theta = 0)$, $A_{yy}(\theta \neq 0)$, and $A_y(\theta \neq 0)$ for $\vec{d} + A \rightarrow \pi(\theta) + X$ reactions were determined in two series of measurements. The first series was performed in a beam of deuterons having a tensor polarization and the momentum of $P_d = 9$ GeV/c, and pions emitted at zero angle ($\theta_\pi = 0$) were detected in it. The results of those measurements were represented in the form of the dependence of the tensor analyzing power T_{20} on the cumulative variable x_c. The dependences of T_{20} on the target mass number and on the sign of the pion charge were studied in addition to the dependence on the pion momentum. The second series of measurements was performed at $\theta_\pi = 135$ and 180 mrad. There, the vector analyzing power $A_y(\theta)$ was measured in addition to the tensor analyzing power $A_{yy}(\theta)$. The results of this series were represented in the form of the dependence on both the cumulative variable x_c and the pion transverse momentum P_t. In that series, the measurements were performed only with a beryllium target.

The results of the measurements were contrasted against the results of calculations performed in the impulse approximation. The first calculations [66, 13]
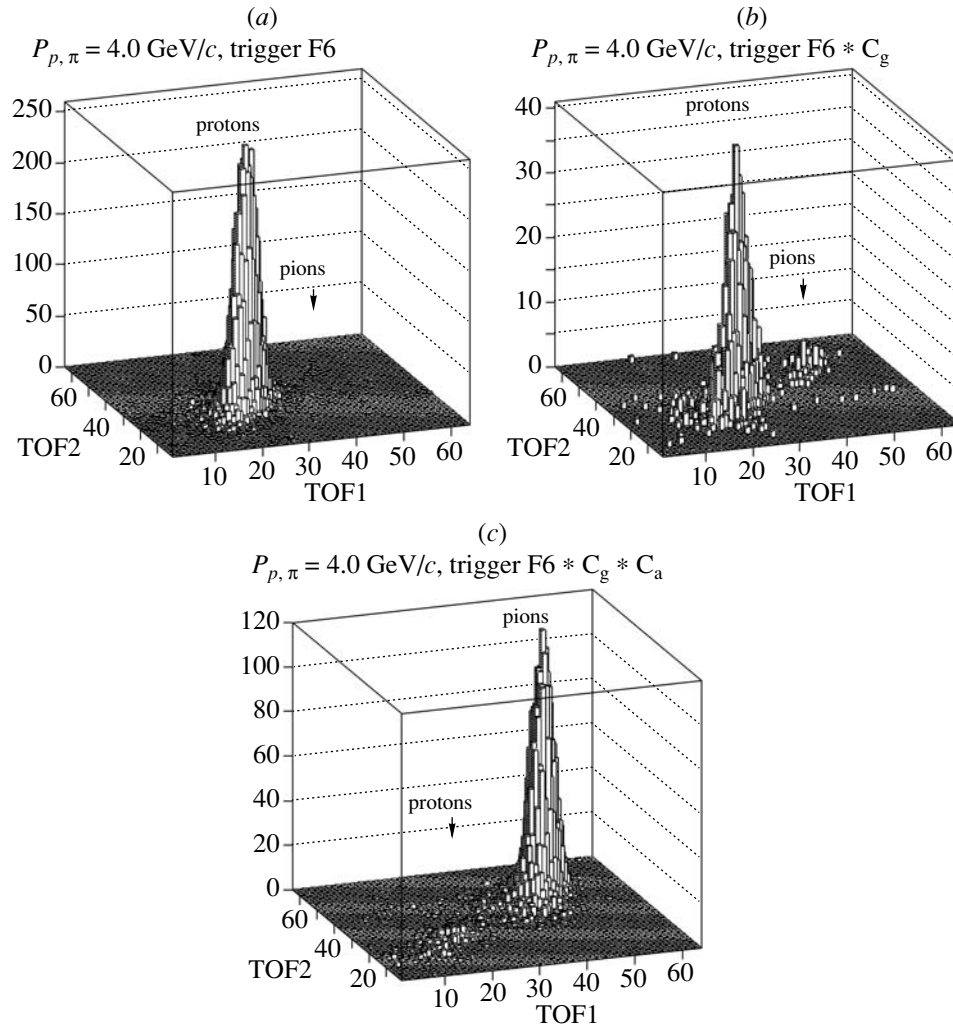
Fig. 5. Correlation time-of-flight spectra (TOF1, TOF2) for secondary particles of momentum 4 GeV/c emitted at an angle of 180 mrad in the fragmentation of 9-GeV/c deuterons. Shown in the figure is the change in the proton-to-pion yield ratio in the spectra for three different triggering conditions: (a) coincidence of signals from the scintillation counters F6$_{1,2,3}$ at the focus F6 (F6 trigger), (b) simultaneous actuation of counters F6$_{1,2,3}$ and the gas counter (F6 $*$ C$_g$ trigger), and (c) simultaneous actuation of counters F6$_{1,2,3}$ and the gas and aerogel counters (F6 $*$ C$_g$ $*$ C$_a$ trigger).

of the internal-momentum (k) dependence of the tensor analyzing power for $\vec{d} + A \rightarrow \pi(0°) + X$ reactions were performed under the assumption that the direct mechanism of cumulative-pion production in the interaction of a deuteron nucleon with a target nucleon, $NN \rightarrow \pi NN$, is dominant. This approach is similar to employing the impulse approximation for $\vec{d} + A \rightarrow p + X$ reactions. The calculations in [13] revealed that the momentum dependence of $T_{20}(k)$ must be similar in the two reactions in question and feature a characteristic minimum in the vicinity of the value of $k \simeq 0.3$ GeV/c (see Fig. 2). At higher values of k, where the reason behind the growing discrepancy between data on T_{20} for $d \rightarrow p$ processes and the results of the calculations in the impulse approximation has yet to be clarified conclusively, a comparison of data

for the two reactions could be helpful in pinpointing the source of these discrepancies.

3.1. Tensor Analyzing Power of Deuteron Fragmentation to Cumulative Pions at Zero Pion Emission Angle

The results of measurement of the analyzing power T_{20} versus the cumulative variable x_c are given in Table 2 and in Fig. 6. Under the assumption of a direct mechanism of pion production, the minimum laboratory internal momentum k_{min} required for the production of a pion with a momentum P_π is unambiguously related to the variable x_c. Table 2 illustrates the relationship between the variables P_π, x_c, and k_{min}.

Table 2. Tensor analyzing power T_{20} in $\vec{d} + A \to \pi(0°) + X$ reactions

P_d, GeV/c	P_π, GeV/c	Target	Δ_t, g/cm^2	x_c	δx_c	$k_{\min}$, GeV/c	$T_{20} \pm$ stat. $\pm$ syst.	σ_{inv}
					π^+ [13]			
9.0	3.0	C	50.4	0.92	± 0.02	–	$0.003 \pm 0.037 \pm 0.001$	–
7.4	3.0	C	50.4	1.23	± 0.03	0.154	$0.120 \pm 0.090 \pm 0.020$	–
					π^- [13]			
9.0	3.0	C	50.4	0.92	± 0.02	–	$-0.002 \pm 0.046 \pm 0.001$	–
8.6	3.0	C	50.4	0.98	± 0.02	0.006	$-0.008 \pm 0.030 \pm 0.001$	–
7.4	3.0	C	50.4	1.23	± 0.03	0.154	$0.051 \pm 0.067 \pm 0.007$	–
7.0	3.0	C	50.4	1.35	± 0.03	0.224	$-0.043 \pm 0.080 \pm 0.006$	–
6.6	3.0	C	50.4	1.49	± 0.03	0.305	$0.210 \pm 0.110 \pm 0.030$	–
6.2	3.0	C	50.4	1.67	± 0.04	0.396	$0.017 \pm 0.138 \pm 0.002$	–
					π^- [67]			
9.0	3.5	H	7.1	1.08	± 0.03	0.051	$0.064 \pm 0.059 \pm 0.004$	23.5
9.0	4.0	H	7.1	1.25	± 0.03	0.155	$0.048 \pm 0.047 \pm 0.003$	19.6
9.0	4.5	H	7.1	1.43	± 0.04	0.270	$0.120 \pm 0.058 \pm 0.008$	3.53
9.0	5.0	H	7.1	1.61	± 0.04	0.392	$0.158 \pm 0.098 \pm 0.010$	0.75
9.0	5.0	Be	36	1.63	± 0.04	0.396	$0.128 \pm 0.056 \pm 0.008$	6.59
9.0	5.3	C	55	1.76	± 0.05	0.520	$0.162 \pm 0.118 \pm 0.010$	1.81

Note: Here, x_c is the cumulative variable; δx_c is width of the x_c interval determined by the spectrometer momentum resolution and the absorption in the target of given thickness Δ_t; P_d and P_π are the laboratory momenta of the deuteron and the pion, respectively; $k_{\min}$ is the internal momentum (see main body of the text); the invariant cross section $\sigma_{\mathrm{inv}} = E_\pi d\sigma/d^3 P_\pi$ is given in μb GeV^{-2} c^3 sr^{-1} nucleon^{-1} units; the uncertainty in σ_{inv} was estimated at 20%; and the systematic uncertainty in T_{20} was due to the uncertainty in the beam polarization.

Measurements of the dependence $T_{20}(x_c)$ were performed in two series. In the first of them [13], the pion momentum $P_\pi = 3.0$ GeV/c was fixed (the tuning of the focusing spectrometer in momentum was not changed), while the momentum of accelerated deuterons was varied in such a way as to cover the interval of x_c values from 0.92 to 1.67. Since detailed investigations of the momentum spectra of cumulative pions revealed that these spectra depend only slightly on the target mass number and are virtually independent of the pion-charge sign [11], we performed all measurements with a carbon target and measurements for unlikely charged pions only for two values of x_c.

Our measurements led to an unexpected result: the values obtained for T_{20} proved to be incompatible in sign and magnitude with the direct-mechanism predictions [13]. An underestimation of secondary pion interactions in carbon nuclei may be the possible reason behind this discrepancy. In the second series, measurements were performed for targets having different mass numbers: carbon, beryllium, and liquid-hydrogen ones [62]. The kinematical scheme of the experiment was also modified with the aim of avoiding losses of time for tuning the accelerator to

a different value of the accelerated-deuteron momentum. The measurements were performed at a single value of $P_d = 9.0$ GeV/c, the range of values of the cumulative variable x_c between 1.08 and 1.76 being covered by changing the momentum tuning of the spectrometer from 3.5 to 5.3 GeV/c [67].

The new measurements confirmed a weak dependence of T_{20} on the target mass number and a monotonic growth of this analyzing power for $x_c > 1$ as the pion momentum becomes higher. The impossibility of describing the data in question on the basis of the direct mechanism, at least without taking into account three-vertex diagrams (final-state interaction), is obvious.

3.2. Tensor Analyzing Power of Deuteron Fragmentation to Cumulative Pions for Nonzero Pion Emission Angles

The mechanisms of rescattering or absorption of the product meson by the second nucleon of the deuteron involved may be responsible for the discrepancy between the results of the calculations in the impulse approximation and data obtained at $\theta_\pi = 0°$.

Table 3. Tensor (A_{yy}) and vector (A_y) analyzing powers in $\vec{d} + \mathrm{Be} \to \pi(\theta) + X$ reactions versus P_t and x_c [68] (the target thickness is $\Delta_\mathrm{t} = 36$ and $29\ \mathrm{g/cm^2}$ for $\theta = 135$ and $180\ \mathrm{mrad}$, respectively)

P_d, GeV/c	P_π, GeV/c	P_t, GeV/c	x_c	k_min, GeV/c	$A_{yy} \pm$ stat. $\pm$ syst.	$A_y \pm$ stat. $\pm$ syst.
$\pi^-, \theta = 135$ mrad						
9.0	2.50	0.366	0.770 ± 0.015	–	$0.111 \pm 0.027 \pm 0.006$	$0.095 \pm 0.028 \pm 0.012$
9.0	3.00	0.404	0.950 ± 0.015	–	$0.011 \pm 0.029 \pm 0.001$	$-0.060 \pm 0.026 \pm 0.007$
9.0	3.50	0.471	1.130 ± 0.015	0.093	$-0.120 \pm 0.054 \pm 0.006$	$0.064 \pm 0.048 \pm 0.008$
9.0	4.00	0.538	1.320 ± 0.015	0.215	$-0.266 \pm 0.078 \pm 0.013$	$-0.038 \pm 0.069 \pm 0.005$
9.0	4.50	0.606	1.520 ± 0.015	0.348	$-0.314 \pm 0.092 \pm 0.016$	$-0.145 \pm 0.080 \pm 0.018$
$\pi^+, \theta = 180$ mrad						
9.0	1.50	0.266	0.446 ± 0.015	–	$-0.024 \pm 0.032 \pm 0.001$	$0.074 \pm 0.014 \pm 0.009$
9.0	2.00	0.354	0.609 ± 0.015	–	$-0.052 \pm 0.034 \pm 0.002$	$0.015 \pm 0.011 \pm 0.002$
9.0	2.50	0.433	0.781 ± 0.015	–	$0.020 \pm 0.034 \pm 0.001$	$0.046 \pm 0.011 \pm 0.006$
9.0	3.00	0.531	0.964 ± 0.015	–	$-0.114 \pm 0.047 \pm 0.006$	$0.039 \pm 0.022 \pm 0.003$
9.0	3.50	0.618	1.157 ± 0.015	0.117	$-0.150 \pm 0.060 \pm 0.008$	$-0.078 \pm 0.024 \pm 0.003$
9.0	4.00	0.708	1.369 ± 0.015	0.250	$-0.438 \pm 0.080 \pm 0.022$	$-0.051 \pm 0.028 \pm 0.003$
$\pi^-, \theta = 180$ mrad						
9.0	1.50	0.226	0.446 ± 0.015	–	$0.056 \pm 0.030 \pm 0.003$	$0.127 \pm 0.015 \pm 0.002$
9.0	2.00	0.354	0.609 ± 0.015	–	$0.005 \pm 0.032 \pm 0.001$	$-0.003 \pm 0.018 \pm 0.001$
9.0	2.50	0.433	0.781 ± 0.015	–	$-0.065 \pm 0.028 \pm 0.003$	$0.049 \pm 0.013 \pm 0.006$
9.0	3.00	0.531	0.964 ± 0.015	–	$-0.068 \pm 0.047 \pm 0.003$	$0.037 \pm 0.019 \pm 0.005$
9.0	3.50	0.618	1.157 ± 0.015	0.117	$-0.148 \pm 0.067 \pm 0.007$	$-0.012 \pm 0.022 \pm 0.003$
9.0	4.00	0.708	1.369 ± 0.015	0.250	$-0.377 \pm 0.071 \pm 0.019$	$0.004 \pm 0.027 \pm 0.001$
9.0	4.50	0.786	1.580 ± 0.015	0.395	$-0.334 \pm 0.105 \pm 0.017$	–
$\pi^-, \theta = 180$ mrad						
5.0	1.45	0.258	1.043 ± 0.015	0.064	$-0.010 \pm 0.052 \pm 0.001$	–
5.0	1.60	0.284	1.180 ± 0.015	0.117	$0.005 \pm 0.054 \pm 0.001$	–
5.0	1.80	0.319	1.370 ± 0.015	0.224	$-0.103 \pm 0.082 \pm 0.005$	–
5.0	2.00	0.354	1.570 ± 0.015	0.316	$-0.107 \pm 0.073 \pm 0.005$	–
5.0	2.10	0.372	1.680 ± 0.015	0.373	$-0.135 \pm 0.107 \pm 0.007$	–
$\pi^-, \theta = 0$						
5.0	1.45	0.0	0.990 ± 0.015	0.045	$0.070 \pm 0.053 \pm 0.003$	–
5.0	1.60	0.0	1.120 ± 0.015	0.107	$0.067 \pm 0.065 \pm 0.003$	–
5.0	1.70	0.0	1.205 ± 0.015	0.149	$0.103 \pm 0.066 \pm 0.005$	–
5.0	1.80	0.0	1.290 ± 0.015	0.171	$0.096 \pm 0.047 \pm 0.005$	–
5.0	2.00	0.0	1.470 ± 0.015	0.276	$0.054 \pm 0.070 \pm 0.003$	–
5.0	2.10	0.0	1.566 ± 0.015	0.324	$0.035 \pm 0.058 \pm 0.002$	–
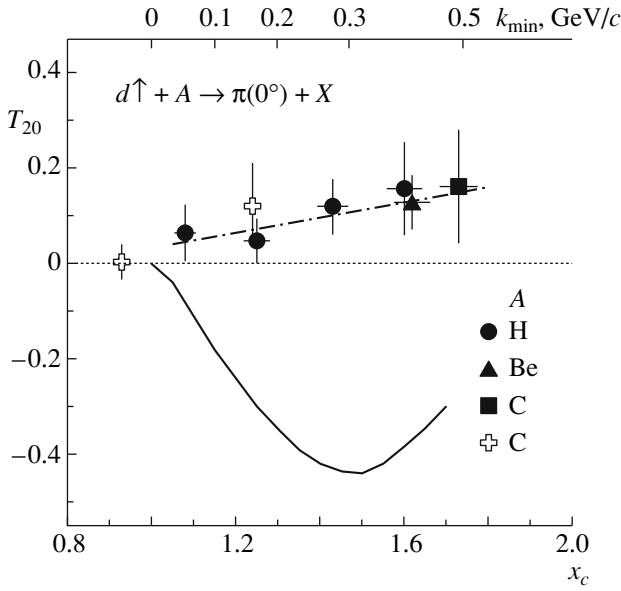
Fig. 6. Tensor analyzing power T_{20} as a function of the cumulative variable x_c in the fragmentation of 9-GeV/c deuterons to pions in $\vec{d} + A \rightarrow \pi^{\pm}(0°) + X$ processes. The closed symbols and open crosses represent data for, respectively, negatively (π^-) and positively (π^+) charged pions. The dash-dotted and solid curves stand for, respectively, an approximation of data by a linear dependence (χ^2/d.o.f. = 0.5) and the result obtained by calculating T_{20} in the impulse approximation [13] with the Paris wave function [41]; $k_{\min}$ is the calculated value of the minimum internal momentum (see main body of the text).

The respective three-vertex diagrams were considered in [47] in interpreting data on the tensor analyzing power T_{20} for deuteron breakup on nuclei in $A(\vec{d}, p)X$ reactions. Estimations revealed that the contribution of this mechanism must decrease as the pion transverse momentum becomes higher. This could be verified by measuring the tensor analyzing power A_{yy} at nonzero pion emission angles.

The respective measurements [68, 69] were performed in a beam of deuterons having a tensor polarization and a momentum of 9.0 GeV/c at pion emission angles of $\theta = 135$ and 180 mrad. A wide range of pion momenta P_{π}, from 1.5 to 4.5 GeV/c, was covered in order to compare the behavior of A_{yy} in the cumulative ($x_c > 1$, $P_{\pi} > 3.1$ GeV/c) and noncumulative ($x_c < 1$) regions. Pion production on quasifree deuteron nucleons is dominant in the noncumulative region. In this case, nucleon–nucleon distances are relatively long, with the result that the D-wave component in the deuteron wave function is small. Since tensor effects are determined by the presence of the D wave in the deuteron wave function, they must be small in the region $x_c < 1$. The results of the measurements are given in Table 3 and in Fig. 7.

In the noncumulative region, the values of A_{yy} are indeed small and are close to those that are observed at zero pion emission angle. In the cumulative region, the tensor analyzing power grows in magnitude, remaining negative, as the pion transverse momentum increases. The dependences $A_{yy}(x_c)$ for positively and negatively charged pions are similar.

It was established experimentally that invariant cross sections for cumulative-pion production, $\sigma_{\mathrm{inv}} \equiv E\frac{d^3\sigma}{dp^3}$, in proton–nucleus interactions [$A(p, \pi)X$] are predominantly dependent on the cumulative variable, but that they are only slightly dependent on the beam energy E_b starting from $E_b \geq 3$ or 4 GeV [10, 11, 17]. If this regularity holds for polarization observables as well, then analyzing powers [in particular, $A_{yy}(x_c)$] must be only slightly dependent on the deuteron momentum at a fixed value of x_c. In order to study the dependence on the fragmenting-deuteron momentum, measurements of A_{yy} were also performed at the lower deuteron momentum of $P_d = 5.0$ GeV/c and pion-emission angles of $\theta_{\pi} = 0$ and 180 mrad [70, 71].

The results obtained by measuring A_{yy} at $P_d = 5.0$ GeV/c are given in Table 3. The dependences $A_{yy}(x_c)$ for $\theta_{\pi} = 0$ and 180 mrad at the deuteron momenta of 5.0 and 9.0 GeV/c are compared in Fig. 8. At $\theta_{\pi} = 0$ and a small value of the tensor analyzing power, its x_c dependences at 5.0 and 9.0 GeV/c are substantially different. In this deuteron-momentum range, A_{yy} changes sign. At $\theta_{\pi} = 180$ mrad, the sign of A_{yy} is conserved, its magnitude being correlated with the value of the pion transverse momentum P_t. The P_t dependence of A_{yy} is shown in Fig. 9. Above a threshold value of $P_t^{\mathrm{thr}} \simeq 0.4$ GeV/c, the dependence $A_{yy}(P_t)$ can be approximated by the linear function $A_{yy} = a + bP_t$, the slope parameter being $b \simeq 1.5$. In comparing the dependence of A_{yy} on the variable x_c, which is correlated with nucleon–nucleon distances in the deuteron, with its dependence on the transverse momentum P_t, which is associated with the transverse component of the relative motion of constituents in the deuteron, one can see that the P_t dependence of A_{yy} is manifestly dominant.

3.3. Vector Analyzing Power A_y of $\vec{p} + A \rightarrow \pi + X$ Reactions for the Case of a Vector Polarization of Deuterons

Measurements of single-spin left–right asymmetries A_y in the fragmentation of high-energy protons having a vector polarization to mesons, $\vec{p} \rightarrow \pi^{\pm}$, [72, 73], revealed two special features: (i) a threshold character of spin effects—that is, $|A_y|$ increases monotonically starting from some values of
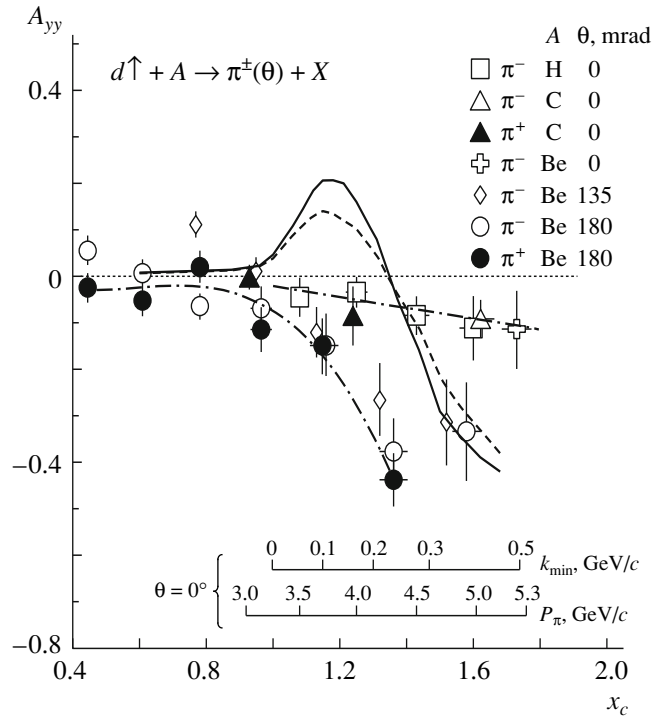
Fig. 7. Analyzing power $A_{yy}(x_c)$ for the fragmentation of deuterons having a tensor polarization and a momentum of 9 GeV/c on hydrogen, beryllium, and carbon targets at pion emission angles of $\theta_\pi = 0$, 135, and 180 mrad. Given for $\theta_\pi = 0$ are the values (in GeV/c units) of the pion momentum P_π and the minimum internal momentum of nucleons in deuterons, k_{min}, in the case of the direct mechanism of pion production ($NN \rightarrow \pi NN$). The solid and dashed curves represent the results obtained for $\theta_\pi = 0$ and 180 mrad, respectively, from calculations performed in the relativistic impulse approximation by using the minimal-relativization scheme [52] and the Reid deuteron wave function [42], while the dash-dotted curves stand for polynomial approximations of the data for $\theta_{\pi\pm}(0)$ and $\theta_{\pi+}$ (180 mrad).
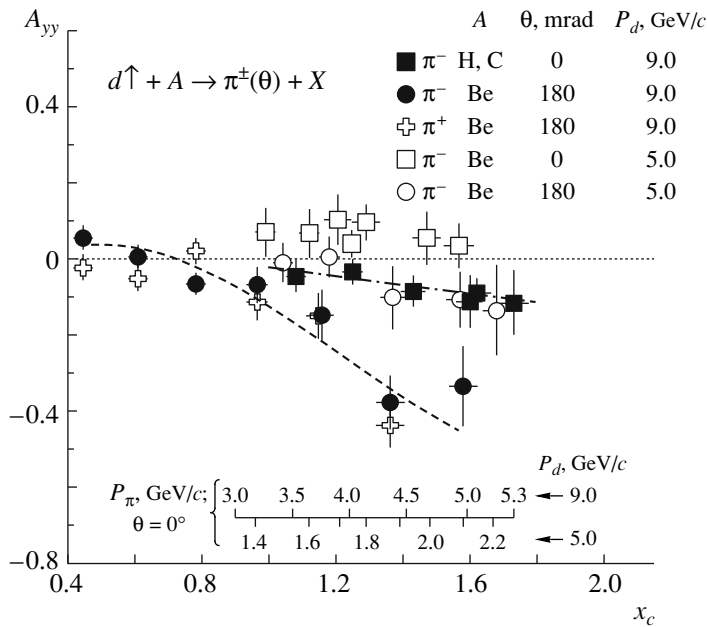
Fig. 8. Analyzing power $A_{yy}(x_c)$ for pion-emission angles of $\theta = 0$ and 180 mrad at the deuteron momenta of $P_d = 5$ and 9 GeV/c. The subsidiary horizontal scale within the picture shows the correspondence between the values of the cumulative variable x_c and the pion momentum P_π at $\theta = 0$ and two values of P_d. The curves represent polynomial approximations of $A_{yy}(x_c)$ at $P_d = 9$ GeV/c for $\theta_\pi = 0$ and 180 mrad.
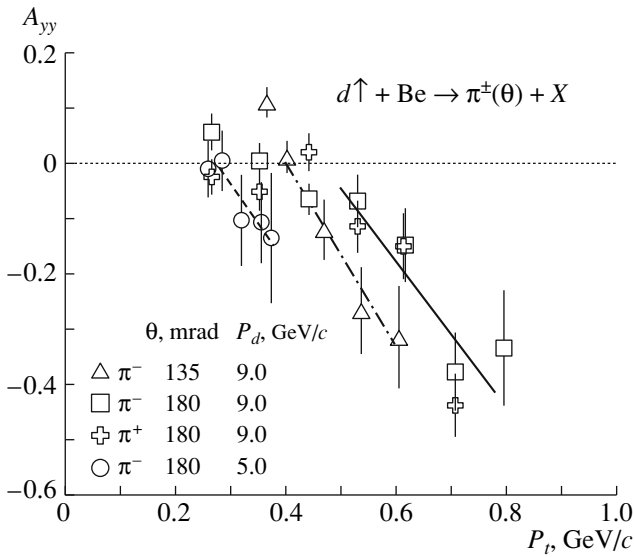
Fig. 9. Tensor analyzing power A_{yy} as a function of the pion transverse momentum P_t. In the cumulative region ($x_c > 1$), $A_{yy}(P_t)$ can be approximated by the linear function $A_{yy} = a_i + b_i P_t$, where the slope parameter takes close values of $b_i \simeq 1.5$ for various values of the deuteron momentum P_d and the pion emission angle θ: (solid line) $P_d = 9$ GeV/c and $\theta = 180$ mrad, (dash-dotted line) $P_d = 9$ GeV/c and $\theta = 135$ mrad, and (dashed line) $P_d = 5$ GeV/c and $\theta = 180$ mrad.

the Feynman variable x_F (about 0.5) and the pion transverse momentum P_t (about 0.5 GeV/c)—and (ii) a correlation between the sign of A_y and sign of the pion charge. This sign correlation is explained in a natural way within the quark-parton mechanism of pion production. In $\vec{p}p$ interaction, pions produced in the region of polarized-proton fragmentation are formed upon the hadronization of one of the leading valence quarks, $u \to \pi^+$ and $d \to \pi^-$. For π^+ mesons, $A_y > 0$, since, in the proton, the direction of the u-quark spin coincides with the direction of the proton spin, while, for π^- mesons, $A_y < 0$ in accordance with the inverse direction of d-quark spin. The threshold effect in the dependences $A_y(x_F, P_t)$ may be associated with a dominant role of the orbital angular momentum of quarks at large x in the formation of the nucleon spin [72].

On the basis of the parton mechanism of the formation of high-momentum pions, one can make the following qualitative predictions. The deuteron is a nucleon pair of zero isospin and contains equal numbers of u and d quarks ($3u$, $3d$). Since a proton–neutron pair in the deuteron is in the spin-triplet state and since the proton and neutron spins are assumed to be correlated in a specific way with the spins of the constituent quarks, $p\uparrow$ ($u\uparrow, u\uparrow, d\downarrow$), $n\uparrow$ ($d\uparrow, d\uparrow, u\downarrow$), four quarks of the six, $2u$ and $2d$, compensate one

another in the formation of left–right pion flows, while the remaining two quarks, u and d, which have identical spin directions ($\uparrow$), form π^+ and π^- mesons characterized by the same sign of the asymmetry $A_y(\vec{d} \to \pi^{\pm}) \simeq \frac{1}{3} A_y(\vec{p} \to \pi^+)$.

Upon going over to the cumulative region ($x_c > 1$), where, as the cumulative variable x_c grows, the D-wave component, in which the orientation of the proton and neutron spins is opposite to the orientation of the deuteron spin, becomes dominant, the sign of A_y must undergo reversal—that is, it becomes negative. The first estimate for the magnitude and momentum dependence of A_y in $\vec{d} + \text{Be} \to \pi^-(\theta) + X$ reactions for $\theta = 135$ mrad was obtained in a beam having a tensor polarization and the momentum of $P_d = 9.0$ GeV/c. For this, use was made of an admixture of the vector component in the beam (see Table 1); according to data from the CH_2 polarimeter, this admixture was $p_z = 0.258 \pm 0.018(\text{stat.})$ upon averaging over the measurement time. The separation of the contributions from the vector and tensor components in calculating A_y is simplified by the fact that the sign of p_z does not change upon the reversal of the sign of the tensor polarization p_{zz} (see Table 1). Despite a relatively poor accuracy of the measurements ($\delta A_y = 0.03-0.08$) because of a small value of the vector component of the deuteron polarization, the measurements at $\theta = 135$ mrad revealed a basic character of the behavior of $A_y(x_c)$ (see Fig. 10): as the pion momentum grows in response to the increase in the cumulative variable x_c from 0.8 to 1.5, A_y decreases from about 0.1 to about -0.1, its sign undergoing reversal upon the transition to the cumulative region.

More precise measurements of A_y with both positively and negatively charged pions [74, 75] were performed with a deuteron beam whose vector polarization is obtained upon switching the ion source used to a purely vector polarization mode (see Table 1, 1−4 and 3−6 high-frequency transitions). In the run with a beam of vector polarization, the polarization p_z was tested at regular intervals by the low-energy polarimeter. A treatment of the data from the polarimeter over the entire period of the measurements (about 60 h) made it possible to approximate the polarization time drift $p_z^{\pm}(T)$ by relations linear in $T(h)$; that is,

$$p_z^+ = (0.550 \pm 0.029) - (0.0016 \pm 0.0012)T,$$

$$p_z^- = (0.457 \pm 0.016) - (0.0017 \pm 0.0007)T.$$

The results of the measurements at six values of the $\pi^{\pm}$ momenta are given in Fig. 10 and in Table 3. Summarizing data on the behavior of $A_y(x_c)$ for π^+ and π^- mesons, one can conclude that the vector
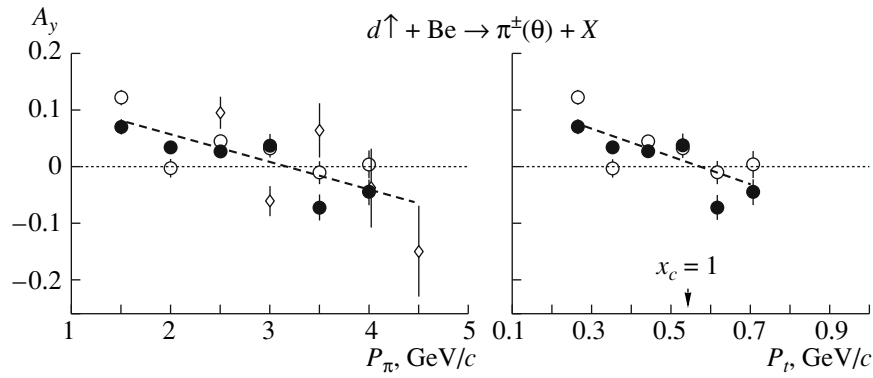
Fig. 10. Vector analyzing power A_y as a function of the total momentum of product pions, P_π, and their transverse momentum, P_t, in the fragmentation of deuterons having a vector polarization and the momentum of 9 GeV/c. The displayed points represent experimental data for (closed circles) π^+ mesons at $\theta = 180$ mrad, (open circles) π^- mesons at $\theta = 180$ mrad, and (open diamonds) π^- mesons at $\theta = 135$ mrad. Linear approximations constructed for the P_π and P_t dependences by using the whole set of experimental points are represented by the dashed lines. The reversal of the sign of A_y occurs at the boundary of the cumulative region ($x_c \simeq 1$).

analyzing power of $\vec{d} \to \pi$ reactions behaves in accordance with expectations following from spin combinatorial analysis for quarks in the proton−neutron system of isospin $I = 0$ and in accordance with the change in the relationship between the contributions of the S and D waves to the deuteron wave function as the nucleon−nucleon distance decreases: (i) A_y has the same sign for π^+ and π^- mesons. (ii) $|A_y|$ is much smaller in deuteron fragmentation ($\vec{d} \to \pi$) than in nucleon fragmentation ($\vec{p} \to \pi$). (iii) As the pion momentum becomes higher, A_y decreases monotonically, changing from positive to negative values upon the transition from the noncumulative ($x_c < 1$) to the cumulative ($x_c > 1$) region, where the contribution of the D wave comes to be dominant.

It should be noted that the threshold behavior of single-spin asymmetries A_y (namely, a fast growth of $|A_y|$ in the region $P_t > P_t^{\text{th}} \simeq 0.5$ GeV/c), which is characteristic of $\vec{p} \to \pi$ processes, is not observed for $\vec{d} \to \pi$ reactions. Under kinematical conditions of the experiment being discussed, the pion transverse momentum of $P_t \simeq 0.5$ GeV/c is close to the boundary where a transition to the cumulative regime occurs and where A_y changes sign. It is of course important to study further the behavior of A_y with a higher precision and at P_t and x_c values larger than those attained in the present experiment. The latter would make it possible to probe the region of higher internal momenta in the deuteron, in which case the nucleon wave functions overlap to a greater extent, so that one would expect stronger manifestations of quark degrees of freedom in the two-nucleon cluster.

4. CONCLUSIONS

The investigation of $\vec{d} + A \to \pi^\pm(\theta) + X$ inclusive reactions that was performed at the Laboratory of High Energies at JINR within the PIKASO (Pion and Kaon Spin Observables) experiment in the beam of polarized deuterons with momenta of up to $P_d = 9$ GeV/c revealed the following:

(i) At $P_d = 9$ GeV/c and $\theta_\pi = 0°$, the tensor analyzing power T_{20} grows monotonically from 0.06 to 0.16 in the pion-momentum range from 3.5 to 5.3 GeV/c ($1.08 \le x_c \le 1.76$). This analyzing power depends only slightly on the target mass number ($A = 1, 9, 12$) and the sign of the pion charge. This behavior of T_{20} is incompatible, both in sign and in magnitude, with the results of the calculations performed in the impulse approximation under the assumption that a dominant contribution comes from the elementary process $NN \to NN\pi$.

(ii) At $P_d = 9$ GeV/c and values of the pion momentum P_π in the range between 1.5 and 4.5 GeV/c ($0.5 \le x_c \le 1.58$), the tensor analyzing power A_{yy} at pion-emission angles of $\theta_\pi = 135$ and 180 mrad exhibits a threshold behavior with respect to the pion transverse momentum P_t: A_{yy} decreases monotonically from values close to zero to -0.4 in the P_t range from 0.4 to 0.8 GeV/c.

(iii) At $P_d = 5$ GeV/c and $\theta_\pi = 180$ mrad, A_{yy} changes insignificantly as x_c increases: $A_{yy} = -0.135$ at $P_t = 0.37$ and $x_c = 1.7$. This can be explained by a small excess of the transverse momentum above the threshold value of about 0.3 GeV/c. A weak dependence of A_{yy} on x_c indicates that, in the case of the parton mechanism of cumulative-pion production on a flucton, the tensor analyzing power depends only slightly on the Bjorken variable x_B (that is, on the

parton longitudinal momentum). The dominance of the P_t dependence suggests of the tensor analyzing power may be a manifestation of the orbital motion of constituents of the deuteron core in the $L = 2$ state (D wave).

(iv) The left−right asymmetry A_y in the fragmentation of tensorially polarized deuterons to pions at $P_d = 9$ GeV/c and $\theta_\pi = 135$ and 180 mrad has been measured over the kinematical region specified by the inequalities $1.5 \leq P_\pi \leq 4.5$ GeV/c and $0.26 \leq P_t^\pi \leq 0.72$ GeV/c. Those measurements revealed that the asymmetry A_y is small and changes monotonically from $A_y \simeq +0.1$ to $A_y \simeq -0.1$ in the cumulative-variable range $0.26 \leq x_c \leq 1.5$, changing sign at $x_c \simeq 1$. A small value of A_y is explained by zero isotopic spin of the deuteron since, in view of the equality of the numbers of u and d quarks in the deuteron, their spin contributions compensate each other to a considerable extent (a similar effect occurs in measuring spin structure functions in deep-inelastic $e\vec{d}$ scattering). The change in sign upon going over from the region $x_c < 1$ to the region $x_c > 1$ is due to the dominance of the D wave in the deuteron-core region ($x_c > 1$), since the direction of the proton and neutron spins in the D wave is opposite to their direction in the S wave.

Thus, the behavior of spin observables in $\vec{d} \to \pi^\pm$ deuteron-fragmentation reactions suggests that, in explaining tensor effects in cumulative meson production on deuterons, it would be natural to rely on treating the deuteron core as a multiquark system with allowance for its spin structure.

Special features that we found experimentally in spin effects show that $A(\vec{d}, \pi)X$ cumulative processes may provide an access to information about the spin structure of fluctons at the level of quark−gluon degrees of freedom. It is of importance to study the fragmentation process for pion-transverse-momentum values in the region $P_t > 0.7$ GeV/c, where $A_{yy}(P_t)$ may approach the regime of saturation. This is expected to furnish additional information about the connection between the fragmentation mechanism and the orbital angular momentum of a neutron−proton flucton. Information about special features of the strange and sea quark components in the neutron−proton flucton and about their role in the formation of the flucton spin structure can be obtained by studying polarized-deuteron fragmentation accompanied by the emission of cumulative charged kaons and vector mesons. An extension of the program of investigations along these lines and its successful implementation hinges upon prospects for increasing the intensity of polarized beams at the accelerator complex of the Laboratory of High Energies at JINR.

REFERENCES

1. L. S. Azhgirei et al., Zh. Eksp. Teor. Fiz. **33**, 1185 (1957) [Sov. Phys. JETP **6**, 911 (1957)].
2. D. I. Blokhintsev, Zh. Eksp. Teor. Fiz. **33**, 1296 (1957) [Sov. Phys. JETP **6**, 995 (1957)].
3. E. Lehman, Phys. Lett. B **62**, 296 (1976).
4. L. L. Frankfurt and M. I. Strikman, Phys. Lett. B **65**, 51 (1976).
5. L. L. Frankfurt and M. I. Strikman, Phys. Lett. B **76**, 285 (1978).
6. A. M. Baldin, Kratk. Soobshch. Fiz. (FIAN), No. 1, 35 (1971).
7. J. Benecke, T. T. Chou, C. N. Yang, and E. Yen, Phys. Rev. **188**, 2159 (1969).
8. R. P. Feynman, Phys. Rev. Lett. **23**, 1415 (1969).
9. V. I. Goldansky, Yu. P. Nikitin, and I. L. Rozental', *Kinematical Methods in High-Energy Physics* (Nauka, Moscow, 1987) [in Russian].
10. A. M. Baldin et al., JINR Commun. No. E1-82-472 (1982), p. 1.
11. V. S. Stavinsky, Fiz. Elem. Chastits At. Yadra **10**, 949 (1979) [Sov. J. Part. Nucl. **10**, 373 (1979)].
12. A. M. Baldin, Nucl. Phys. A **434**, 695 (1985).
13. S. Afanasiev et al., Nucl. Phys. A **625**, 817 (1997).
14. J. D. Bjorken, Phys. Rev. **179**, 1547 (1969).
15. Yu. D. Bayukov et al., Yad. Fiz. **20**, 59 (1974) [Sov. J. Nucl. Phys. **20**, 30 (1974)].
16. E. Moeller et al., Phys. Rev. C **28**, 1246 (1983).
17. I. M. Belyaev et al., Yad. Fiz. **56** (10), 135 (1993) [Phys. At. Nucl. **56**, 1378 (1993)].
18. S. Frankel et al., Phys. Rev. C **20**, 2257 (1979).
19. N. A. Nikiforov et al., Phys. Rev. C **22**, 700 (1980).
20. M. I. Strikman and L. L. Frankfurt, Fiz. Elem. Chastits At. Yadra **11**, 515 (1980) [Sov. J. Part. Nucl. **11**, 198 (1980)].
21. L. L. Frankfurt and M. I. Strikman, Phys. Rep. **160**, 235 (1988).

22. V. K. Lukyanov and A. I. Titov, Fiz. Elem. Chastits At. Yadra **10**, 815 (1979) [Sov. J. Part. Nucl. **10**, 321 (1979)].

23. V. V. Burov, V. K. Lukyanov, and A. I. Titov, Fiz. Elem. Chastits At. Yadra **15**, 1249 (1984) [Sov. J. Part. Nucl. **15**, 558 (1984)].

24. European Muon Collab. (J. J. Aubert et al.), Phys. Lett. B **123**, 275 (1983).

25. L. L. Frankfurt and M. I. Strikman, Phys. Rept. **76**, 215 (1981).

26. A. F. Efremov et al., Yad. Fiz. **57**, 932 (1994) [Phys. At. Nucl. **57**, 874 (1994)].

27. V. K. Lukyanov, B. L. Reznik, and A. I. Titov, Soob-shch. OIYaI (JINR) No. R2-79-12754 (1979).

28. BCDMS Collab., Preprint No. E1-93-133, JINR (Dubna, 1993).

29. CCFR Collab. (M. Vakili et al.), Phys. Rev. D **61**, 052003 (2000).

30. CLAS Collab. (K. S. Egiyan et al.), Phys. Rev. Lett. **96**, 082501 (2006).

31. R. Schiavilla et al., Phys. Rev. Lett. **98**, 132501 (2007).

32. T. Aono et al., Phys. Rev. Lett. **74**, 4997 (1995).

33. L. S. Azhgirey et al., Phys. Lett. B **387**, 37 (1996).

34. C. F. Perdrisat, Phys. Rev. Lett. **59**, 2840 (1987).

35. V. Punjabi et al., Phys. Rev. C **39**, 608 (1989).

36. V. Punjabi et al., Phys. Lett. B **350**, 178 (1995).

37. L. S. Azhgirey et al., Phys. Lett. B **391**, 22 (1997).

38. A. A. Nomofilov et al., Phys. Lett. B **325**, 327 (1994).

39. B. Kuehn et al., Phys. Lett. B **334**, 298 (1994).

40. E. Cheung et al., Phys. Lett. B **284**, 210 (1992).

41. M. Lacombe et al., Phys. Lett. B **101**, 139 (1981).

42. R. V. Reid,Jr. , Ann. Phys. (N.Y.) **50**, 411 (1968).

43. R. Machleidt, K. Holinde, and Ch. Elster, Phys. Rep. **149**, 1 (1987).

44. R. Machleidt, Phys. Rev. C **63**, 024001 (2001).

45. V. G. J. Stoks et al., Phys. Rev. C **49**, 2950 (1994).

46. A. P. Kobushkin and L. Vizireva, J. Phys. G **8**, 893 (1982).

47. G. I. Lykasov, Fiz. Elem. Chastits At. Yadra **24**, 140 (1993) [Phys. Part. Nucl. **24**, 59 (1993)].

48. A. P. Kobushkin, Phys. Lett. B **421**, 53 (1998).

49. A.P. Kobushkin, Yad. Fiz. **62**, 1213 (1999) [Phys. At. Nucl. **62**, 1140 (1999)].

50. L. P. Kaptari et al., Phys. Lett. B **404**, 8 (1997).

51. W. W. Buck and F. Gross, Phys. Rev. D **20**, 2361 (1979).

52. A. Yu. Illarionov, A. G. Litvinenko, and G. I. Lykasov, Czech. J. Phys. **51** (Suppl. 1), A307 (2001).

53. W. Lakin et al., Phys. Rev. **98**, 139 (1955).

54. L. J. B. Goldfarb, Nucl. Phys. **7**, 622 (1958).

55. H. H. Barshall and W. Haeberli, in *Proceedings of the 3rd International Symposium on Polarization Phenomena in Nuclear Reactions, Madison, USA, 1970* (Wisconsin Univ., Madison, 1971), p. XXV.

56. W. Haeberli, in *Nuclear Spectroscopy and Reactions*, Ed. by J. Cherny (Academic Press, New York, 1974).

57. V. P. Ershov et al., in *Proceedings of International Workshop on Polarized Beams and Polarized Gas Target, Cologne, Germany, 1995*, p. 193.

58. Yu. K. Pilipenko, V. M. Slepnev, and L. S. Zolin, in *Proceedings of the Spin Physics Symposium (SPIN'2000), Osaka, Japan, 2000*, p. 800.

59. V. G. Ableev et al., Nucl. Instrum. Methods Phys. Res. A **306**, 73 (1991).

60. V. Chazikhanian et al., Phys. Rev. C **43**, 1532 (1991).

61. L. S. Azhgirey et al., Nucl. Instrum. Methods Phys. Res. A **437**, 340 (2003).

62. Yu. T. Borzunov et al., Prib. Tekh. Eksp., No. 3, 31 (1984).

63. I. M. Belyaev et al., Soobshch. OIYaI (JINR) No. R1-87-489 (1987).

64. R. Brun et al., *GEANT Users Guide, volume Entry W5013 of CERN Program Library* (Geneva, Switzerland, 1994).

65. L. S. Zolin et al., Kratk. Soobshch. OIYaI (JINR) No. 2[88]-98 (1998), p. 27.

66. M. V. Tokarev, in *Proceedings of the International Workshop Dubna Deutron'91, Dubna, Russia, 1991*, Preprint No. E2-92-25, JINR (Dubna, 1992), p. 84.

67. S. V. Afanasiev et al., Phys. Lett. B **445**, 14 (1998).

68. L. Zolin et al., Nucl. Phys. A **689**, 414c (2001).

69. S. Afanasiev et al., in *Proceedings of International Nuclear Physics Conference (INPC 2001), Berkeley, California, USA, 2001*, p. 395.

70. L. S. Zolin et al., in *Proceedings of 17th International IUPAP Conference on Few-Body Problems in Physics, Durham, North Carolina, USA, 2003* (Elsevier, 2004), p. S240.

71. L. Zolin et al., in *Proceedings of the 16th International Spin Physics Symposium (SPIN'2004), Trieste, Italy* (World Sci., Singapore, 2005), p. 565.

72. Zuo-Tang Liang and C. Boros, Int. J. Mod. Phys. A **15**, 927 (2000).

73. S. B. Nurushev and M. G. Ryskin, Phys. At. Nucl. **69**, 133 (2006).

74. S. Afanasiev et al., Nucl. Phys. A **721**, C645 (2003).

75. L. Zolin (for the SPHERE Collab.), in *Proceedings of the XI Advansed Research Workshop on High Energy Spin Physics, Dubna, Russia, 2005* (JINR, Dubna, 2006), p. 480.

Translated by A. Isaakyan